Response to Review Comments of the Second Reviewer

Dear Reviewer and Editors:

We are sincerely grateful to the editor and reviewer for their valuable time for reviewing our manuscript. The comments are very helpful and valuable, and we have addressed the issues raised by the reviewer in the revised manuscript. Please find our point-by-point response (in blue text) to the comments (in black text) raised by the reviewer. We have revised the paper according to your comments (highlighted in red text of the revised manuscript).

Sincerely yours,

Dr. Yuanjian Yang, representing all co-authors

Major comments:

1. Section 2.3.1: The HW definition requires stronger justification. Specifically, why did the authors decide to use reference stations to define HW and why was the threshold set to "more than two reference stations"?

Response: We apologize for the unclear in the original manuscript regarding the HW events definition. We have supplemented relevant details in the revised version to address this issue.

Reference stations (primarily rural stations) provide a baseline of regional climatic conditions unaffected by urbanization, ensuring that the defined HWs reflect true regional extreme HW events rather than local CUHI effects. As highlighted in previous studies (Cheng et al., 2020; Stewart & Oke, 2012), rural reference stations, with minimal impervious surfaces and anthropogenic heat emissions, capture the natural climatic background.

Heat waves, by nature, are large-scale extreme weather events (Perkins et al., 2012;

Rajulapati et al., 2022), and a single reference station's abnormal high temperatures may result from local factors (e.g., microtopography, temporary human activities) rather than a true regional HW. Requiring confirmation from multiple reference stations reduces the risk of misclassification due to individual station errors or local anomalies, improving the robustness of the definition. This aligns with the statistical logic in our study, where HW were counted independently at each station but required spatial consistency to be recognized as a regional event (Xue et al., 2023).

In summary, using reference stations ensures the HW definition is rooted in regional climatic anomalies, while the multi-station threshold guarantees the spatial generality of the identified heat waves, making the results more reliable for analyzing CUHI and HW.

References:

Cheng, X., Lan, T., Mao, R., Gong, D., Han, H., Liu, X.: Reducing air pollution increases the local diurnal temperature range: a case study of Lanzhou, China, Meteorological Applications, 27, https://doi.org/10.1002/met.1939, 2020.

Perkins, S. E., Alexander, L. V., & Nairn, J. R.: Increasing frequency, intensity and duration of observed global heatwaves and warm spells, Geophysical Research Letters, 39, https://doi.org/10.1029/2012GL053361, 2012.

Rajulapati, C. R., Gaddam, R. K., Nerantzaki, S. D., Papalexiou, S. M., Cannon, A. J., Clark, M. P.: Exacerbated heat in large Canadian cities, Urban Climate, 42, 101097, https://doi.org/10.1016/j.uclim.2022.101097, 2022.

Stewart, I. D., & Oke, T. R.: Local climate zones for urban temperature studies, Bulletin of the American Meteorological Society, 93, 1879–1900, https://doi.org/10.1175/BAMS-D-11-00019.1, 2012.

Xue, J., Zong, L., Yang, Y., Bi, X., Zhang, Y., Zhao, M.: Diurnal and interannual variations of canopy urban heat island (CUHI) effects over a mountain–valley city with a semi-arid climate, Urban Climate, 48, 101425, https://doi.org/10.1016/j.uclim.2023.101425, 2023.

2. Section 2.3.3: More details on the training/validation processes of XGBoost are needed. How were the collinearity among morphological indicators (e.g.,

FAR and BCR) treated in the ML models? More detailed explanations of SHAP and PDP methods would improve reader comprehension of the results in Figure 6-8.

Response: Thank you for your constructive comments. We appreciate the opportunity to clarify the methodological details, and we have supplemented Section 2.3.3 with additional explanations as follows:

(1) Details on the training/validation processes of XGBoost:

The XGBoost model training and validation processes were designed to ensure robustness:

"In this study, we first performed iterative calculations on 7 commonly used hyperparameters (eta, gamma, max_depth, min_child_weight, subsample, colsample_bytree, and nrounds) within a preset hyperparameter tuning space, and selected the optimal hyperparameter combination that minimizes model error using a 5-fold cross-validation method (Yang et al., 2020; Lin et al., 2024). After completing hyperparameter optimization, we randomly split the sample points in the Yangtze River Basin at a 7:3 ratio to obtain training samples (70%) and validation samples (30%), which were used for training and validating the XGBoost model, respectively. Meanwhile, the coefficient of determination (R^2) and root mean square error (RMSE) were chosen as evaluation metrics for simulation accuracy. "

Reference:

Lin, Z., Xu, H., Han, L., et al.: Day and night: Impact of 2D/3D urban features on land surface temperature and their spatiotemporal non-stationary relationships in urban building spaces, Sustainable Cities and Society, 108, 105507, https://doi.org/10.1016/j.scs.2024.105507, 2024.

Yang, L., Xu, H., & Yu, S.: Estimating PM2.5 concentrations in Yangtze River Delta region of China using random forest model and the Top-of-Atmosphere reflectance, J. Environ. Manag., 272, 111061, 2020.

(2) Treatment of collinearity among morphological indicators:

To address collinearity among morphological indicators in the XGBoost model, we first conducted a correlation analysis for feature screening, following established methodologies in similar studies (Harrell, 2015). Specifically, pairwise Pearson

correlation coefficients were calculated for all indicators, with a threshold of 0.8 set to identify highly collinear features. Features exceeding this threshold were evaluated for retention based on their physical significance and relevance to CUHII. For FAR (Floor Area Ratio) and BCR (Building Coverage Ratio), their correlation coefficient was 0.56, well below the 0.8 threshold, indicating moderate correlation without severe collinearity. Thus, both indicators were retained in the model.

Notably, the correlation coefficient between H (average building height) and H-std (building height standard deviation) exceeded 0.8. Both are critical urban morphological parameters influencing the local thermal environment (Tian et al., 2019), yet their regulatory mechanisms differ substantially. On one hand, taller buildings reduce daytime surface temperatures by increasing shading and reducing solar radiation input at the surface (Zhang et al., 2016; Krayenhoff & Voogt, 2016; Taleghani et al., 2016; Cai, 2017). Conversely, high-rise buildings have higher heat capacity, enabling heat storage and slow nighttime release, which delays cooling and intensifies nocturnal heat island effects (Unger, 2004). Additionally, ventilation resistance increases with H: taller buildings strongly block air flow, potentially causing stagnant air in the urban canopy and localized heat accumulation (Hang et al., 2011). In contrast, H-std (building height standard deviation) captures height variation, reflecting spatial heterogeneity of urban morphology with distinct thermal regulatory roles. By day, greater H-std enhances urban canopy turbulence, promoting air circulation and heat dissipation to reduce LST. For instance, studies in Shenzhen show significant cooling when ln(H-std) > 0.5, as increased height variation strengthens surface roughness and airflow disturbance (Wan et al., 2025). Similarly, Fuzhou's BH_std (building height standard deviation) correlates negatively with daytime LST, indicating ventilation-driven cooling (Lin et al., 2024). Given their distinct roles in regulating thermal environments, H and H-std are irreplaceable. Therefore, this study retained both indicators.

Reference:

Harrell, F. E. Regression Modeling Strategies: With Applications to Linear Models, Logistic and Ordinal Regression, and Survival Analysis (2nd ed.), Springer, https://doi.org/10.1007/978-3-319-19425-7, 2015.

Tian, Y., Zhou, W., Qian, Y., Zheng, Z., & Yan, J.: The effect of urban 2D and 3D morphology on air temperature in residential neighborhoods, Landscape Ecology, 34(5), 1161–1178, https://doi.org/10.1007/s10980-019-00834-7, 2019.

Unger, J.: Intra-urban relationship between surface geometry and urban heat island: review and new approach, Climate Research, 27, 253–264, https://doi.org/10.3354/cr0272532004, 2004.

Zhang, H., Zhu, S., Gao, Y., Zhang, G.: The relationship between urban spatial morphology parameters and urban heat island intensity under fine weather condition, Journal of Applied Meteorological Science, 27, 2, 249–256. https://doi.org/10.11898/1001-7313.20160213, 2016.

Krayenhoff, E. S., Voogt, J. A.: Daytime thermal anisotropy of urban neighbourhoods: Morphological causation, Remote Sensing, 8, 2, https://doi.org/10.3390/rs8020108, 2016.

Taleghani, M., Sailor, D., Ban-Weiss, G. A.: Micrometeorological simulations to predict the impacts of heat mitigation strategies on pedestrian thermal comfort in a Los Angeles neighborhood, Environmental Research Letters, 11, 2, https://doi.org/10.1088/1748-9326/11/2/024003, 2016.

Cai, H., Xu, X.: Impacts of built-up area expansion in 2D and 3D on regional surface temperature, Sustainability, 9, 10, https://doi.org/10.3390/su9101862, 2017.

Hang, J., Li, Y., Sandberg, M.: Experimental and numerical studies of flows through and within high-rise building arrays and their link to ventilation strategy, Journal of Wind Engineering & Industrial, 99, 1036–1055, https://doi.org/10.1016/j.envsoft.2016.06.021, 2011.

Wan, Y., Du, H., Yuan, L., Xu, X., Tang, H., & Zhang, J.: Exploring the influence of block environmental characteristics on land surface temperature and its spatial heterogeneity for a high-density city, Sustainable Cities and Society, 118, 105973, https://doi.org/10.1016/j.scs.2024.105973, 2025.

Lin, Z., Xu, H., Yao, X., Yang, C., & Ye, D.: How does urban thermal environmental factors impact diurnal cycle of land surface temperature? A multi-dimensional and multi-granularity perspective, Sustainable Cities and Society, 101, 105190, https://doi.org/10.1016/j.scs.2024.105190, 2024.

(3) Detailed explanations of SHAP and PDP methods :

Explainable machine learning techniques can help understand the prediction process

of "black-box models", as well as how the relationships between variables change within their value ranges (Bansal & Quan, 2024). Such post-hoc explanation techniques can probe into the model to reveal the relationships between variables. We have expanded the descriptions of SHAP to enhance clarity:

"SHAP (SHapley Additive exPlanations): This method quantifies each feature's contribution to individual predictions based on Shapley values from game theory (Park et al., 2023). For each sample, SHAP values decompose the prediction into feature-specific contributions, with positive/negative values indicating promotion/inhibition of CUHII. "

In addition, Partial Dependence Plot (PDP) is a commonly used technique that can present the marginal effects of independent variables (Friedman, 2001). The generated plots show partial dependence function values, which are the average marginal effects on the prediction results. The partial dependence function is defined as follows:

$$\hat{f}_s(x_s)=E_{x_c}[\hat{f}(x_s,x_c)]=\int \hat{f}(x_s,x_c)dP(x_c) \quad (1)$$

Where$x_s$is the target feature whose effects are to be studied, x_c are other marginalized features, and P represents the marginal probability density. The function $\hat{f}_s$ can be estimated using the Monte Carlo approximation method, with the formula as follows:

$$\hat{f}_s(x_s)=\frac{1}{n}\sum_{i=1}^{n}\hat{f}\left(x_S,x_C^{(i)}\right) \quad (2)$$

where $x_C^{(i)}$ denotes the value of x_c in the dataset, and n is the sample size.

Due to the model-agnostic nature of the above PDP specification, it can be applied to both traditional linear regression models and machine learning models such as XGBoost. For linear models, PDP can present marginal effects when other independent variables take their mean values; for machine learning models, PDP can present the relationships between variables based on the tree structure of the model (Bansal & Quan, 2024).

To address this, we have supplemented the derivation and core meaning of PDP to enhance clarity:

"Partial dependency plots (PDP) are a common explainable machine learning technique that reveals the marginal effect of a target feature (e.g., urban

morphological indicators) on prediction outcomes (CUHII) by holding other features at their average levels or marginalizing their effects (Friedman, 2001; Bansal & Quan, 2024). Specifically, PDP illustrates the average trend of change in CUHII as a single indicator (or a combination of two indicators) varies, while other indicators remain stable—thereby isolating the independent impact of the target indicator. By leveraging PDP to visualize the functional relationship between feature variables and model outputs, we clarify the marginal effects of urban morphological indicators on CUHII, which supports the identification of key driving factors and their threshold characteristics. "

These supplementary ensure the methodological rigor of the ML-based analyses and improve the interpretability of results in Figures 6–8. We appreciate your guidance in strengthening the methodological transparency of our study.

Reference:

Park, S., Park, J., Lee, S.: Unpacking the nonlinear relationships and interaction effects between urban environment factors and the urban night heat index. Journal of cleaner production, 428, https://doi.org/10.1016/j.jclepro.2023.139407, 2023.

Bansal, P., Quan, S. J.: Examining temporally varying nonlinear effects of urban form on urban heat island using explainable machine learning: A case of Seoul, Building and Environment, 247, 1.1–1.20, https://doi.org/10.1016/j.buildenv.2023.110957, 2024.

Friedman, J. H.: Greedy Function Approximation: A Gradient Boosting Machine, Annals of Statistics, 29(5), 1189–1232, https://doi.org/10.2307/2699986, 2001.

3. Section 3.2: Before presenting the analysis of Figures 6-8, there should be at least one figure showing the model performance of XGBoost, as the validity of these results strongly depend on the model's predictability of CUHII.

Response: Thank you for this valuable suggestion. We fully agree that verifying the predictive performance of the XGBoost model is critical to supporting the validity of subsequent analyses (Figures 6–8).

To address this, we have added a new figure (now Figure X, placed at the beginning of Section 3.2) that demonstrates the model's performance. This figure includes: (1) a

scatter plot of observed vs. predicted CUHII values, with a fitted regression line; (2) statistical metrics such as R^2, RMSE, and MAE to quantify prediction accuracy. These results confirm that the XGBoost model achieves robust predictability, providing a reliable basis for the subsequent SHAP and partial dependency analyses.

We appreciate your insight, which has enhanced the rigor of our methodological validation.

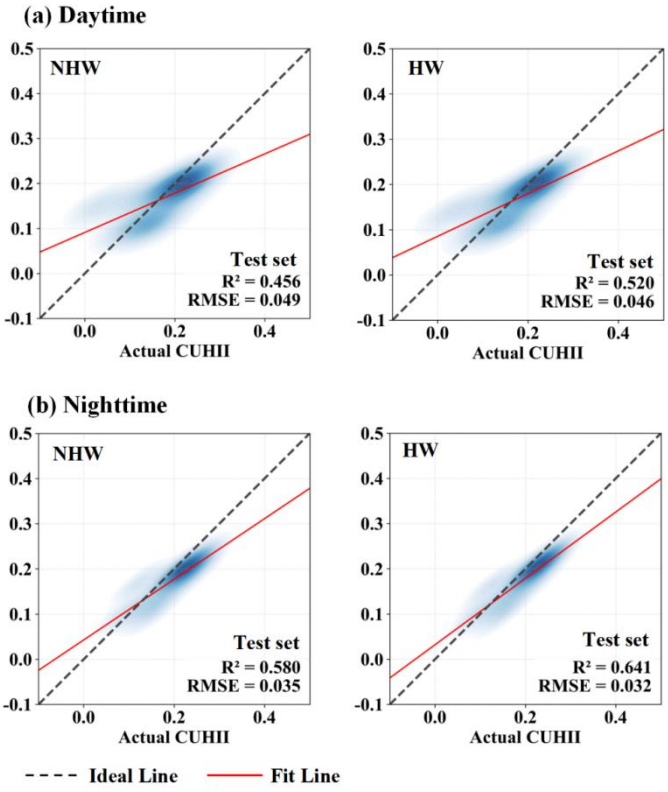

Figure S1: The performance graph of the XGBoost model in predicting CUHII.

4. Line 255-257: This summary largely repeats content in line 236-239. The authors should streamline the conclusion from figure 8, e.g., focus more on the nonlinear modulation.

Response: We apologize for the redundant in the previous version. We have deleted the content in lines 236–239 to avoid repetition. Based on the findings from Figure 8, we have streamlined the conclusion regarding nonlinear modulation. The revised description is as follows:

"In summary, the regulation of urban morphology on CUHII exhibits significant

diurnal asymmetry: 2D indicators predominate during the daytime, while 3D indicators play a dominant role at night. Furthermore, urban morphology exerts nonlinear modulation on CUHII, characterized by threshold effects and dual roles (e.g., SVF showing both negative and positive impacts), with these nonlinear effects being more pronounced during HW periods."

5. Section 3.3: The scenario setup requires clarification. How were the uniform SVF values applied across the entire domain in scenario II and III? Does scenario I have spatially heterogeneous SVF values? If so, the rationale for using uniform values in scenario II and III needs justification. Currently it is difficult to interpret spatial changes in Figures 10-13 with most discussions focused on the central point.

Response: Thank you for your valuable comment. We apologize for the insufficient clarification on scenario setup and spatial characteristics of SVF, which has led to difficulties in interpretation. We have revised the relevant content to address these concerns, and the key explanations are as follows:

(1) SVF characteristics in Scenario I: Scenario I adopted the original building heights of the study area (a 500-meter radius around Station 651061), where building heights vary spatially due to real urban morphological heterogeneity (e.g., differences in residential and commercial building heights). Consequently, the SVF in Scenario I is spatially heterogeneous, with local variations around the mean value of 0.76, reflecting the actual urban spatial pattern.

(2) Uniform adjustment of SVF in Scenarios II and III: To isolate the independent effect of SVF on thermal environment, we adjusted building heights uniformly across the entire domain in Scenarios II and III (while keeping street width, building footprint, and BCR unchanged). This uniform adjustment ensured that SVF values in these scenarios are more spatially consistent (targeting 0.735 and 0.685, respectively), reducing interference from other spatial heterogeneities (e.g., uneven building height distribution). This design allows us to explicitly link temperature changes to SVF variations, avoiding confounding effects from concurrent changes in multiple

morphological factors.

(3) Enhanced spatial analysis: We agree that analyzing only the central point temperature is insufficient to reflect spatial variations, and we apologize for the oversimplified interpretation. To address this, we have supplemented spatial heterogeneity analysis of temperature responses across the entire domain, rather than focusing solely on the central point. In addition, we have merged Figures 10 and 11, Figures 12 and 13 to facilitate the comparison of diurnal and nocturnal characteristics under different simulation scenarios. The revised content is as follows:

"The figure above shows the simulated AT spatial distribution under different scenarios during daytime (Figure 10a). Spatial patterns reveal that during NHW periods, Scenario II shows a 0.2–0.7°C temperature rise across the study region. The central point confirms this trend, with AT increasing from 30.68℃ in Scenario I to 31.09℃ in Scenario II. Meanwhile, Scenario III exhibits a 0.3–0.8°C cooling in these areas, driven by building shadows, with the central point AT in Scenario III decreasing to 30.33°C. During HW periods, these effects intensify. Scenario II sees a 0.5–1.1°C warming across these zones, with the central point air temperature in Scenario II increasing from 35.01℃ to 35.76℃. Scenario III shows a 0.6–1.4°C cooling in study region, with the central point AT in Scenario III dropping to 34.39℃. As SVF decreased, the obstruction of building clusters to air flow intensified, reducing the heat dissipation capacity. Meanwhile, blocking of long wave radiation was exacerbated, promoting heat accumulation and leading to temperature increases. It should be noted that the temperature change patterns in Scenario III, like the drop in central point AT, are related to excessively low SVF significantly increasing building shadow areas, enhancing the shading effect on solar radiation, thus reducing surface heat absorption and inhibiting temperature rise (Perini & Magliocco, 2014). Figure 10b shows the spatial distribution of the simulated AT indifferent scenarios at night. During NHW periods, the central point AT in Scenario I was 24.86℃, increasing to 25.10℃ in Scenario II with a relatively small variation, while that in Scenario III increased significantly to 25.90℃. During HW periods, the central point AT in Scenario I was 26.25℃, increasing to 26.83℃ in Scenario II and increased

significantly to 27.93℃ in Scenario III. Notably, this pattern of temperature variation (moderate rise in Scenario II, sharp increase in Scenario III) is consistent across the entire simulation domain. The increase in building height hinders the convective heat dissipation of nighttime air, making heat dissipation difficult and thus promoting a significant temperature rise (Mo et al., 2024). Furthermore, the temperature differences between the scenarios during the HW periods were more significant than during the NHW periods, indicating that changes in building height have a more pronounced impact on air temperature during the HW periods, further amplifying the non-linear modulation of the building SVF in AT."

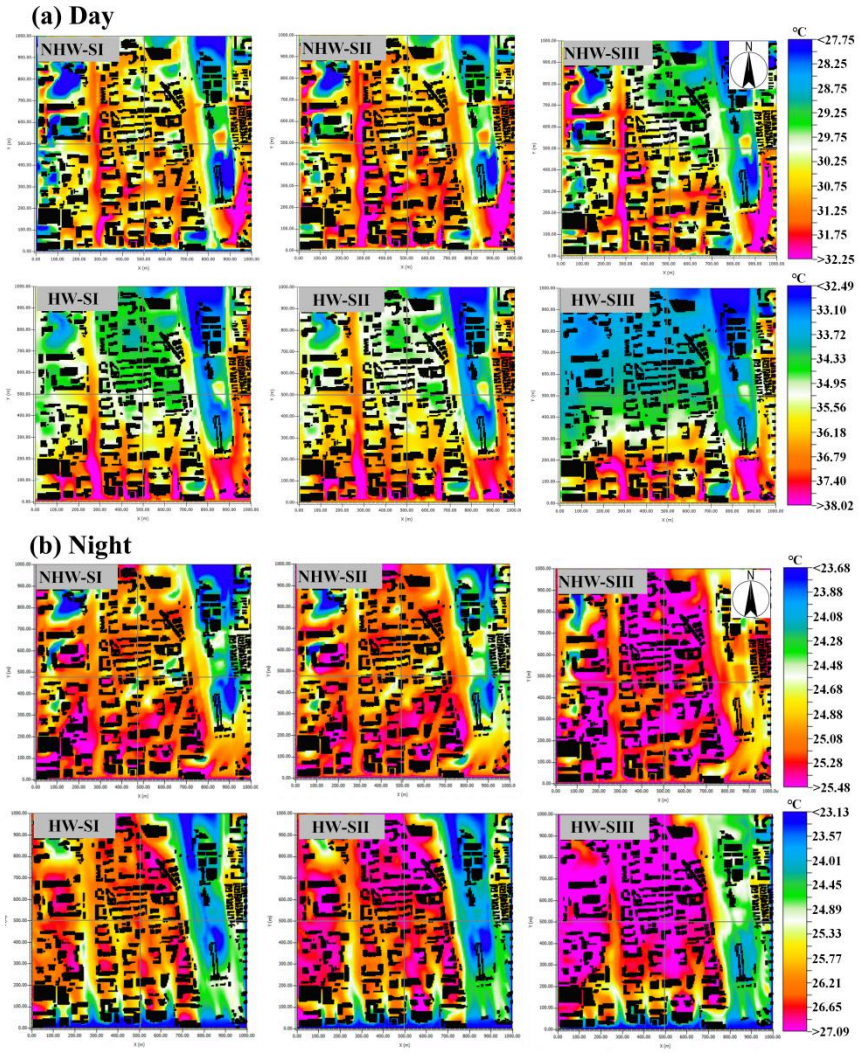

Figure 10: Spatial distributions of simulated AT across scenarios during daytime (a) and nighttime (b). NHW-SI represents Scenario I during NHW periods, HW-SI represents Scenario I during HW periods, and so forth. The intersection of the two gray crosshairs in each subplot indicates the

location of the meteorological station.

“Combined with the spatial distribution of short-wave (SW) radiation, the temperature phenomena under different SVF daytime conditions can be further explained (Figure 11a). Overall, SW radiation during HW periods is higher than during NHW periods. Specifically, in Scenario II during the HW periods, the average SW radiation slightly decreases from 636.16 W/m² to 602.27 W/m², the SW radiation at the central point decreases from 970 W/m² to 930 W/m², but AT shows an upward trend. This can be attributed to the obstruction of air flow by buildings (Ge et al., 2025), where the heat accumulation effect dominates in the competition between SW radiation attenuation caused by increased building height and air flow resistance. In Scenario III, the average SW radiation drops to 537.88 W/m², the central point’s SW radiation plummets to 860 W/m², and significant shadow shading leads to a substantial reduction in SW radiation (Lin et al., 2024), thereby inhibiting the temperature rise. At night, the heat dissipation of LW radiation exhibits stronger non-linear threshold characteristics (Figure 11b). In Scenario II during the HW periods, the average LW radiation increases from 408.34 W/m² to 412.81 W/m², and the LW radiation at the central point climbs from 388 W/m² to 394 W/m². At this time, the resistance to escape of LW radiation is limited, so the air temperature only increases slightly. In Scenario III, the lower SVF significantly reduces the loss of LW radiation to the atmosphere, with the average LW radiation rapidly increasing to 424.31 W/m², and the central point’s LW radiation surges to 410 W/m², accompanied by a noticeable temperature increase. This is because multiple reflections between building facades retain radiation energy within urban canyons, thus enhancing the capture of LW radiation (Mei et al., 2025). In summary, buildings exert nonlinear modulation on urban diurnal thermal environments through the competitive effects of SW radiation shading and ventilation resistance, as well as the reflection and accumulation mechanisms of LW radiation.”

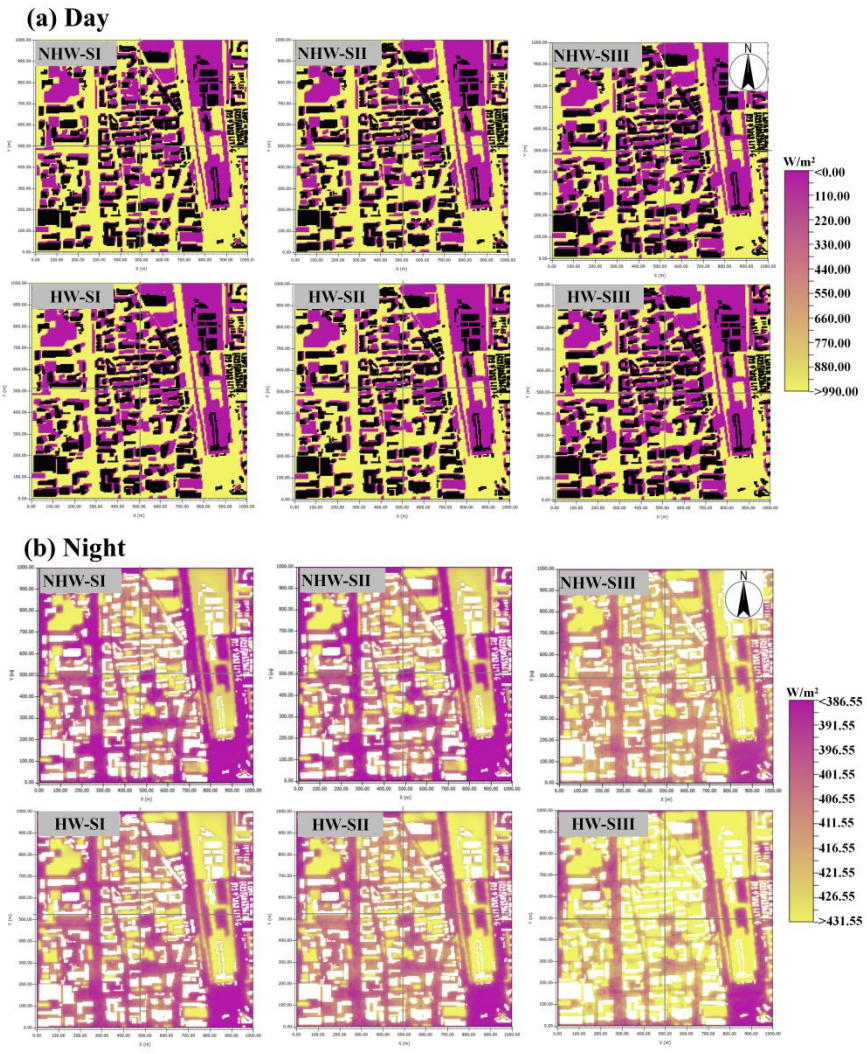

Figure: 11 Spatial distribution of simulated short-wave (SW) radiation (a) and long-wave (LW) radiation (b) across scenarios during NHW and HW periods.

6. Section 4: While the wind-CUHII relationship is worth discussing, the analysis should emphasize how urban morphology modulates wind patterns to be tightly connected with the main theme of this work. The current presentation of Figures 14-16 lacks clear connection to morphological controls, making it difficult to identify the key messages.

Response: Thank you very much for your valuable comments, which have helped us identify critical issues in our discussion. We sincerely apologize for the unclear presentation in Section 4. We have carefully revised this section to address these concerns, and the key explanations are as follows:

“Figure 12a shows that during the daytime, the correlation coefficients (r) between WS and CUHII were -0.14 during NHW periods and -0.18 during HW periods, indicating a weak negative correlation that was slightly stronger during HW periods. Deng et al. (2025) simulated that a 10% increase in WS could reduce the CUHII by 0.16℃ during summer days. Stronger solar radiation during HW periods makes the heat dissipation effect of wind more significant for CUHII. During the night (Figure 12b), the r was -0.19 during NHW periods and -0.27 during HW periods, with enhanced negative correlations compared to daytime, especially during HW periods. This may be related to the heat dissipation characteristics of the underlying urban surface during nighttime (Liu et al., 2022), where slower heat release makes the modulation of WS in CUHII more pronounced. Notably, compared with research findings from other cities (Yang et al., 2023; Rajagopal et al., 2023; Deng et al., 2025), the CUHII in Beijing exhibits a unique characteristic—it is insensitive to WS variations both during the daytime and nighttime. This phenomenon may be closely linked to urban morphology and local geographical environments. Urban morphology significantly modulates wind penetration and heat exchange efficiency: compact built-up areas with high BCR and low SVF (e.g., the Second Ring Road) form dense building clusters that block airflow, reducing WS and weakening wind-driven heat dissipation, thus making CUHII less responsive to WS changes. In addition, existing studies have confirmed that local circulations formed under different geographical backgrounds can significantly reshape the spatiotemporal distribution of urban extreme high temperatures (Zhang et al., 2011; Zhou et al., 2020; Chen et al., 2022). Specifically for Beijing, the mountainous terrain in its western and northern regions gives rise to a typical mountain-valley wind circulation, which interacts with urban morphology: dense buildings in central areas disrupt valley breeze penetration, while sparse layouts in suburbs align with mountain winds. This interplay between morphology and terrain-induced winds weakens the modulation of WS variations on CUHII. Observations show that wind directions in Beijing’s urban area display a regular diurnal variation: northerly winds (mountain breeze) dominate from 05:00 to 10:00 Beijing Time; there is an obvious reversal around 11:00, shifting to southerly

winds (valley breeze) which persist until 04:00 the next day. Additionally, the average WS of the mountain breeze is significantly lower than that of the valley breeze (Zheng et al., 2018). Such distinct periodic characteristics make mountain-valley breeze a key local factor influencing Beijing's thermal environment (Dou et al., 2014). Based on this, we speculate that the "insensitivity of CUHII to WS variations" observed in this study may be the result of interactions between the mountain-valley breeze cycle, urban morphology, and the inherent diurnal cycle of CUHII."

In short, the coupling mechanism between local circulation, urban morphology and the diurnal cycle of CUHII (Fig. R1) may hold the key to explaining how WS acts on CUHII. We will further quantify this mechanism through refined numerical simulations in future research.

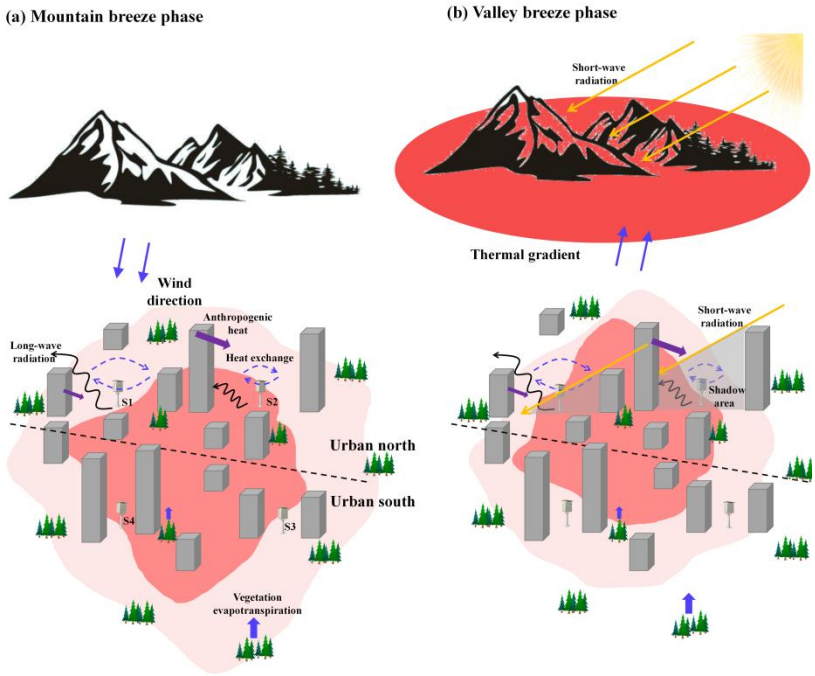

Figure R1: Schematic diagram illustrating the modulation of CUHII by mountain-valley breeze (self-draw).

"Urban ventilation corridors represent an energy-efficient ecological approach to improving urban wind-thermal environments by taking advantage of natural meteorological conditions (Masmoudi & Mazouz, 2004; Masson, 2006; Palusci et al., 2021). In recent years, Beijing has proposed to construct ventilation corridors to alleviate increasingly severe urban environmental problems, with corridor designs intentionally aligned with urban morphological features—such as low BCR, high SVF,

and wide street canyons—to minimize aerodynamic resistance (Figure 13a). This section designates nine stations within first-level ventilation corridors (VC-Stations) as those embedded in open built-up areas (sparse buildings, low-rise structures) and the remaining 39 stations in compact built-up areas (NVC-Stations) as Non-Ventilation Corridor Stations. Data show that WS at NVC-Stations (Figure 13b) is significantly lower than that at VC-Stations (Figure 13c), a difference primarily driven by urban morphological controls: dense high-rises in NVC areas disrupt airflow, while VC areas' open layouts allow unobstructed wind penetration. For example, at night during HW periods, WS at NVC-Stations remains around 0.5 m/s due to wind blockage by closely packed buildings, whereas that at VC-Stations stays above 0.8 m/s, facilitated by their low-rise, sparse morphologies. CUHII in VC-Stations generally exhibits an inverse relationship with WS, with morphological traits amplifying this effect. At NVC-Stations, their compact morphologies (high BCR, low SVF) limit heat dissipation; when WS is 0.5 m/s in the early morning during HW periods, CUHII reaches 1.9℃ due to trapped heat. In contrast, when WS increases to 1.5 m/s in the afternoon at VC-Stations—where open morphologies enhance turbulent heat exchange—CUHII drops to only 0.3℃. Notably, the CUHII mitigation effect of ventilation corridors shows significant diurnal differences influenced by urban morphology. During the daytime, high baseline WS reduces the relative impact of ventilation corridor-induced WS gains, but VC areas' low-rise structures still promote more efficient heat dispersion than NVC's dense canyons. During nighttime, with lower background WS, the WS enhancement from VC's open morphologies is more pronounced (Hsieh & Huang, 2016), and the thermal environment—sensitive to trapped heat in NVC's compact morphologies—is more responsive to WS modulation (She et al., 2022), resulting in significantly lower nighttime CUHII at VC-Stations (42.09% lower during NHW periods and 33.91% lower during HW periods)."

These revisions strengthen the connection between urban morphology and wind-CUHII dynamics, ensuring the analysis is tightly linked to our focus on urban morphology's role in modulation of CUHI.

Reference:

Chen, S., Yang, Y., Deng, F., Zhang, Y., Liu, D., Liu, C., Gao, Z.: A high-resolution monitoring approach of canopy urban heat island using a random forest model and multi-platform observations, Atmospheric Measurement Techniques, 15, 735–756, https://doi.org/10.5194/amt-15-735-2022, 2022.

Dou, J., Wang, Y., Miao, S.: Fine spatial and temporal characteristics of humidity and wind in Beijing urban area, Journal of Applied Meteorological Science, 25, 5, 559–569, https://doi.org/10.11898/1001-7313.20140505, 2014.

Miao, Y., Liu, S., Chen, B., Zhang, B., Wang, S., Li, S.: Simulating urban flow and dispersion in Beijing by coupling a CFD model with the WRF model, Advances in Atmospheric Sciences, 30, 6, 1663–1678, https://doi.org/10.1007/s00376-013-2234-9, 2013.

Rajagopal, P., Priya, R. S., & Senthil, R.: A review of recent developments in the impact of environmental measures on urban heat island, Sustainable Cities and Society, 88, 104279, https://doi.org/10.1016/j.scs.2022.104279, 2023.

Zhang, N., Zhu, L. F., Zhu, Y.: Urban heat island and boundary layer structures under hot weather synoptic conditions: A case study of Suzhou City, China, Advances in Atmospheric Sciences, 28, 4, 855–865, https://doi.org/10.1007/s00376-010-0040-1, 2011.

Zheng, Z., Ren, G., Gao, H.: Analysis of the local circulation in Beijing area, Meteorological Monthly, 44, 3, 425–433, https://doi.org/10.7519/j.issn.1000-0526.2018.03.009, 2018.

Zhou, X., Okaze, T., Ren, C., Cai, M., Mochida, A.: Evaluation of urban heat islands using local climate zones under the influences of sea-Land breeze, Sustainable Cities and Society, 55, 102060, https://doi.org/10.1016/j. scs.2020.102060, 2020.

Masmoudi, S., & Mazouz, S.: Relation of geometry, vegetation and thermal comfort around buildings in urban settings, the case of hot arid regions, Energy and Buildings, 36(7), 710–719, https://doi.org/10.1016/j.enbuild.2004.01.043, 2004.

Palusci, O., Monti, P., Cecere, C., Montazeri, H., & Blocken, B.: Impact of morphological parameters on urban ventilation in compact cities: the case of the Tuscolano-Don Bosco district in Rome, Science of The Total Environment, 807, 150490, https://doi.org/10.1016/j.scitotenv.2021.150490, 2022.

Hsieh, C. M., & Huang, H. C.: Mitigating urban heat islands: A method to identify potential wind corridor for cooling and ventilation, Computers Environment and Urban Systems, 57, 130–143, https://doi.org/10.1016/j.compenvurbsys.2016.02.005, 2016.

She, Y., Liu, Z., Zhan, W., et al.: Strong regulation of daily variations in nighttime surface urban heat islands by meteorological variables across global cities, Environmental Research Letters, 17(1), 014049, https://doi.org/10.1088/1748-9326/ac4630, 2022.

Minor comments:

1. Figure 3: There are (a)-(f) in the caption but only four subplots are presented.

Response: We apologize for the error in Figure 3 where the caption incorrectly. This has been corrected to ensure the number of subplots matches the caption. We have also thoroughly reviewed the entire manuscript to prevent similar issues in other figures. Thank you for bringing this to our attention.

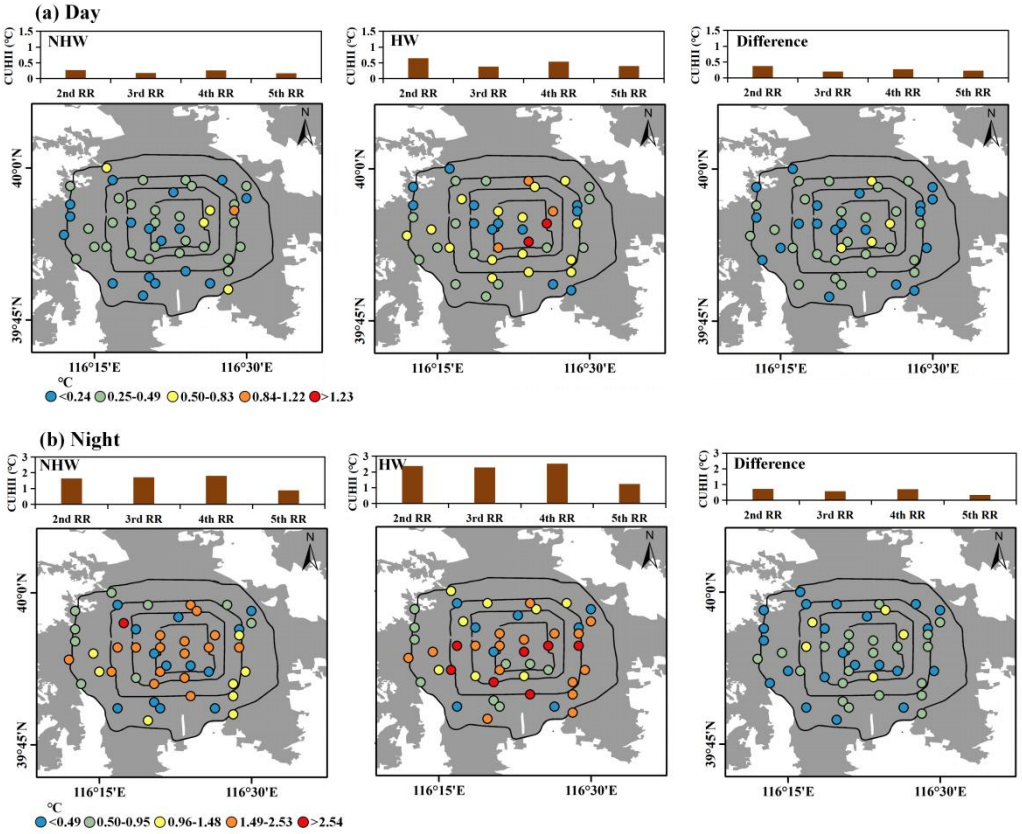

Figure: 3 Diurnal spatial patterns of CUHII during NHW & HW. Panel (a) for daytime, (b) for nighttime. In each panel, left: NHW CUHII stats & distribution; middle: HW CUHII stats & distribution; right: HW-NHW CUHII difference.

2. Figure 6: It would be easier to interpret if the authors can group 2D and 3D indicators (e.g.presenting all 2D indicators in the first 6 rows, followed by 3D indicators).

Response: We apologize for the unclear differentiation of 2D and 3D urban morphological indicators in Figure 6, which compromised interpretability. The current arrangement of indicators in the SHAP plots follows the feature importance order automatically determined by the XGBoost model (based on their contribution to CUHII predictions), resulting in the interleaving of 2D (e.g., BCR, L/W) and 3D (e.g., H, SVF, H-std) indicators.

Recognizing the merit of your suggestion, we have enhanced the figure by color-coding 2D indicators in red and 3D indicators in green. Thank you for your constructive feedback, which has guided us to strengthen the figure's communicative clarity.

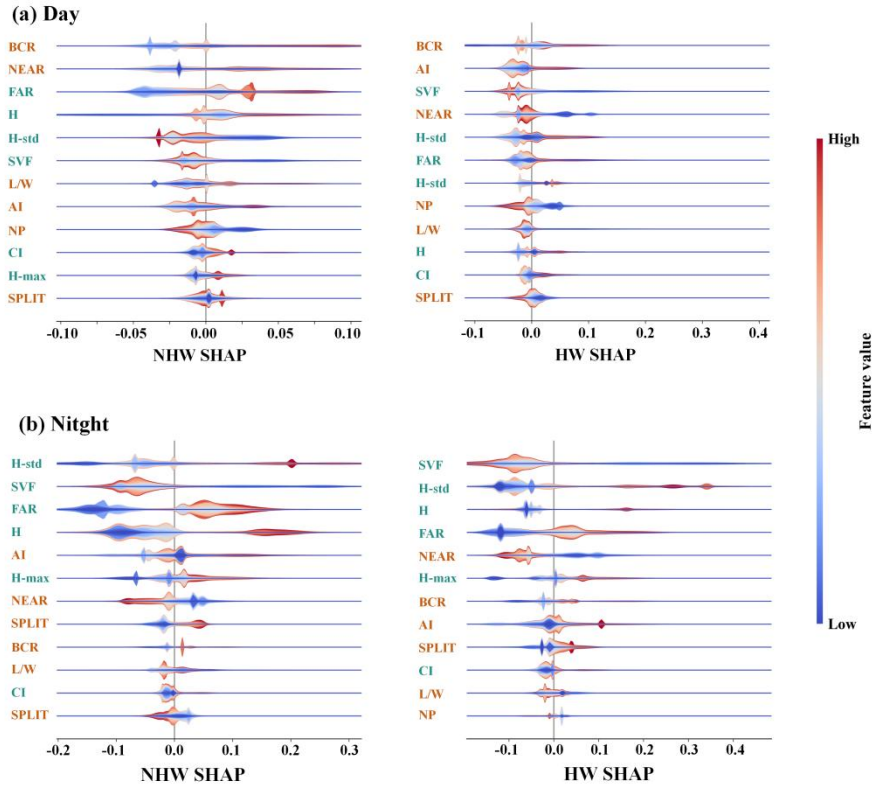

Figure 6: SHAP value analysis of urban morphology indicators for diurnal CUHII during NHW and HW periods, using XGBoost model. SHAP quantifies feature contributions to model outputs. The red/blue color gradients represent high/low feature values, with red indicating 2D urban morphological indicators and green indicating 3D

urban morphological indicators.

3. Figure 9d: Does the 'simulation accuracy' refer to scenario I?

Response: We apologize for the ambiguous reference to "simulation accuracy" in Figure 9d. To address this, we have explicitly clarified in the figure caption. The updated caption now states: "(d) simulation accuracy of air temperature (AT) for Scenario I during NHW and HW periods."